Satyendra Nath Mandal *et al*, International Journal of Advances in Agricultural Science & Technology,
Vol.9 Issue.4, April-2022, pg. 8-26

ISSN: 2348-1358
Impact Factor: 6.901
NAAS Rating: 3.77

Early Possible Detection of Downy Mildew in *Cucumis sativus'* through Hyperspectral Image Analysis

Satyendra Nath Mandal[1]; Subhranil Mustafi[2]; Shubhajyoti Das[3]; Sanket Dan[4]
[1]Kalyani Government Engineering College, satyen_kgec@rediffmail.com
[2]Kalyani Government Engineering College, subhranilmustafi2011@gmail.com
[3]Kalyani Government Engineering College, dasshubhajyoti@gmail.com
[4]Kalyani Government Engineering College, sanketdan@gmail.com

DOI: 10.47856/ijaast.2022.v09i04.002

Abstract

Hyperspectral Imaging has become an important method in monitoring vegetation and crops and producing information regarding onset of diseases. The availability of spectrometers in the market is not only costly but also requires standard-operating-procedures in using them. The use of Specim IQ, a handheld spectrometer with a wavelength-captivating-range of 400-1000 nm has been found to be optimistic in field-application with least complexity. In this paper, an early possible detection of downy mildew has been analysed through the difference in spectral distribution patterns through the reflectance-wavelength graph so that the well-advanced result may avert any significant damage over the visual eyes.

Keywords: Hyperspectral Imaging, Specim IQ, NDVI, PRI, Plant Vegetation, Spectral Indices

1. Introduction

As the world population is increasing rapidly (following the net growth rate = (births-deaths)/size of the population * 100), feeding such a population has become a matter of serious concerns for scientists and administrators. To add pie to the cake, agricultural lands, water for irrigation and other resources are getting limited with passing days. Now, producing crops with the least damage has become one of the most important key factors for successful utilization and feeding the population. To gain such a milestone, the factors and diseases that destroy crops are primarily needed to be identified and get them eradicated. To pursue such operations, several farmers, termed as 'crop scouts' have been hired and periodically sent to fields to inspect the crops and apply for pesticides in case of discrepancies. However, this event of spraying pesticides happens after when the disease gets tracked and within that time, a significant number of crops get utterly damaged, eventually resulting in the least usefulness. Also, the main objective of precision agriculture is to precisely use pesticides and other chemicals since it affects the ecological balance in the food chain and excess spraying or

© 2022, IJAAST All Rights Reserved, https://ijaast.com/

ISSN: 2348-1358
Impact Factor: 6.901
NAAS Rating: 3.77

unnecessary spraying of pesticides and other chemicals before the actual onset of diseases, result in degradation of the quality of the yield and several physiological problems upon consumption.

To identify the specific point where the disease has already arrived but has still not produced any damage such as downy mildew or downy mildew visually, the behaviour towards internal distortions inside the crops needs to be studied thoroughly. Since, humans can identify any object after when light reflects from that surface (i.e., reflectance) in red, green and blue bands primarily, the reflectance in other wavelength bands might be crucial to be analysed in order to decipher such phenomena. To divide the visual and near-infrared spectrum into finer bands, a non-imaging spectrometer has been used has a range of 400-1000 nm, popularly termed as a hyperspectral camera.

The primary difference between multispectral and hyperspectral camera is the number of bands the camera can split into (i.e., spectral resolution) (Fig.1). In the case of multispectral imaging, the bands get divided into 10 finer bands (Ahmed et al., 2016) and division into finer bands for more than 10 is usually served by hyperspectral cameras. Since, the hyperspectral camera that has been used here can divide into 204 different wavelengths, internal distortions inside the body of the crop before the visual exposure may easily be captured in any of the wavelengths using the property of reflectance over the spectral signatures. Due to such high spectral resolution of hyperspectral images, it becomes easier to address the timely detection of the physiological status of the crop itself (Gonzalez-Dugo et al., 2015; Lucieer et al., 2014).

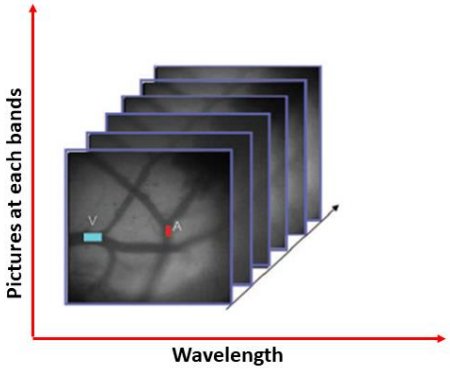

Fig. 1: Spatial and Spectral Division of Hyperspectral Image into split bands (Fong & Wachman, 2008)

Despite the higher accuracy and throughput of hyperspectral imaging, over the past few decades, it has not been extensively used in monitoring agricultural land commercially. It is due to the cost of deploying the applications and the camera itself and few other technical challenges such as low signal-to-noise ratio and large data volume (Darvishzadeh et al., 2012; Hruska et al., 2012; Lodhi et al., 2019; Transon et al., 2018). Here, in hyperspectral imaging, the output is collectively termed as data cube since it contains rows*columns*224 wavelength information rather than only row*column*3 for RGB imaging. To overcome such difficulties several miniaturized and low-cost hyperspectral sensors have been developed and used in significant fields such as Nano and Micro-Hypespec (Headwall Photonics Inc.), FireflEYE (Cubert GmbH, Ulm, Germany), HySpex VNIR (HySpex, Norway), etc. These cameras can be attached to any manned or unmanned aerial platforms such as UAVs, Helicopters, Airplanes to monitor and survey over a particular area at a distance but with high accuracy of resolution (Gonzalez-Dugo et al., 2015; Lu et al., 2020). Data Analysis in such

© 2022, IJAAST All Rights Reserved, https://ijaast.com/

ISSN: 2348-1358
Impact Factor: 6.901
NAAS Rating: 3.77

technological advances regarding the portability of such sensors has gathered a wide recognition in the domain of non-destructive and quality assessment of crops (Caballero et al., 2020).

Use of the Spectral Vegetation Indices helps in identifying the physiology of plants and certain parameters such as chlorophyll content (Blackburn, 1998; Gitelson et al., 2002; Penuelas et al., 1995), pigment, the content of water(PEÑUELAS et al., 1993) and the area of the leaf (Rouse J.~W. et al., 1974). Although the indices lack disease specificity, several factors and experiments prove that vegetation indices based on spectral signatures play a major role in identifying the area and possibility of the disease being affected (Hatfield et al., 2008; Thenkabail et al., 2000). It has also been shown by many researchers about the capability of spectral signatures in identifying the disease of crops (Doraiswamy et al., 2003; Galvão et al., 2009). (Huang et al., 2007; Mahlein et al., 2012; Steddom et al., 2005)It has been stated the value proposition of spectral indices in the prediction of fungal diseases.

This study presents an automatic classification of downy mildew disease in Cucumber with later advances in early detection. The Virus Pseudoperonospora cubensis cause serious damage to the upper surface of the old leaves especially in cucurbits and such results in a loss of AUD 7.3 million per year, annually (Taylor & Cook, 2018). (Bravo et al., 2003), identified the difference between the spectral reflectance between the healthy and unhealthy wheat plants to estimate the extent of damage caused. 5 Pots of healthy Cucumber plants have been used to estimate the spectral signatures in different wavelengths and later those were inoculated with pathogens at a relative humidity of 65-75% at a temperature of 30-35°C in a plant growth chamber to obtain the spectral signatures of the respective coordinates to identify the difference in the measurement due to the damage by the external pathogens on the crops.

Hence, Contributions through this paper can be inferred as follows:

1. Novelty in Early Detection of Downy Mildew in *Cucumis sativus* through hyperspectral imaging.
2. Gradation of the levels of diseases and specific selection of spectral bands for each.
3. Developing a suitable supplication model for the handheld spectrometer for taking and instantaneous analyzing of diseases in crops near future.

The paper has been broadly divided as follows: introduction in Section 1 followed by Materials and Methods in Section 2, Methodology in Section 3, Result and Discussion in Section 4 and Conclusion and Future Work in Section 5.

2. Materials & Methods

2.1 Components of Hyperspectral Images

There are a number to images backing the methodology in capturing spectral images through spectrometers and hyperspectral cameras. The most common method in capturing the image is through the usage of push broom scanners where the light gets separated into different wavelengths through the convex grating. This separation is then recorded in a light sensitive chip. The camera or object is then moved in capturing the next line, satisfying to be called as push broom scanner. In this paper, the applications of such method and camera have been restricted to the identification and calculation of spectral indices of the vegetation with detection of earliest possible symptom for downy mildew.

© 2022, IJAAST All Rights Reserved, https://ijaast.com/

ISSN: 2348-1358
Impact Factor: 6.901
NAAS Rating: 3.77

The images adhering to such restrictions have been captured both in indoor (Laboratory) and outdoor (Farmer's field) lighting conditions. Laboratory setup includes the use artificial ambient light and outdoor setup consists the outdoor natural illumination of the sunlight for capturing the spectral signatures. There are a number of factors which affect the illumination are, the surface of object, day time, shadows from clouds and other factors contributing to secondary illumination onto the region of interest. Hence, detection of key wavelengths should be focused primarily along with subsidiaries in calculating the desired output based on the objective.

As we know healthy leaves reflect more in NIR region compared to the VIS region, hence analyzing the types of leaves becomes easier in the range of 700-1000 nm with spectral resolution of 7nm (Fig.2).

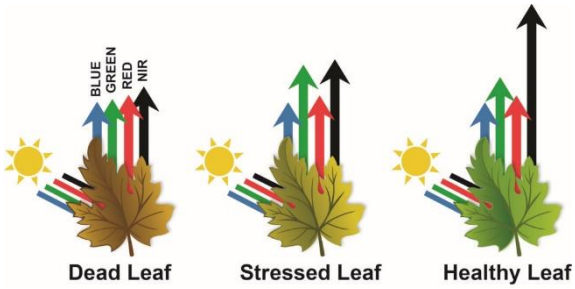

Fig 2.: Leaf types and reflectance at respective spectra (*Credit: https://midopt.com/healthy-crop/*)

2.2 Dataset collection from field cultivation

Cucumber plants (*Cucumis sativus*) have been grown in plastic pots (Fig. 1) (ø 14 cm) under the conditions of controlled temperature (23°C) and humidity (90%) in an artificial plant growth chamber where the lighting conditions have been mechanised to be on from 6 am to 5 pm and off thereafter. Artificial pathogen inoculation has been served by spraying through a plastic bottle where the disease has been centrifuged using Vortex homogenizer under the speed control range of 500-3000 rpm following the process of vigorous resuspension of cells. Seven plants have been kept in the clay pots (ø 35 cm) in the rooftop garden of Kalyani Government Engineering College, Kalyani-741235, India for the natural onset of diseases from the environment. However, a systematic study of samples from healthy to slightest onset of disease being affected has been procured from Chasarhati farmer's field (Coordinates 22.9884712, 88.4294802) Kalyani-741235, India.

2.3 Measurement of the Leaf Reflectance

The reflectance from the leaves has been measured using a handheld hyperspectral camera, Specim IQ (Behmann et al., 2018). The spectral range of the spectrometer is 400-1000 nm covering a maximised portion of visible, NIR and SWIR wavelength bands divided into 204 different wavelengths with the image resolution being 512 X 512 px and spectral resolution being 7 nm (Table 1). Artificial lamps have been placed under indoor image acquisition setup to illuminate the object in getting the maximised reflectance values and increase the quality and homogeneity of spectral data at a particular point in time. The reflectance values are seen to be less than 1 after performing instrument calibration prior to the experiment. A solid plate of barium sulphate has been used as a white reference for marginalising the data from maximum and minimum reflectance values

© 2022, IJAAST All Rights Reserved, https://ijaast.com/

ISSN: 2348-1358
Impact Factor: 6.901
NAAS Rating: 3.77

(100% and 0% respectively). An integration time of 5-8ms has been set and adjusted due to the internal light source wherein values greater than it would incorporate the high probability of noise in the image thus degrading the quality thereafter.

Table 1: Specim IQ Specification (Behmann et al., 2018)

Camera interface	USB Type-C
Connectivity of Camera	GPS
Size of Camera	207 X 91 X 74 mm (depth with lens 125.5 mm)
Weight	1.3 kg
F/number	1.7
Wavelength range	400–1000 nm
Spectral resolution	FWHM 7 nm
Slit length	42 µm
Slit height of the camera	11.7 mm
Spatial sampling	512 px
Spectral bands for the camera	204
Image dimension	512 X 512 px
Data output of file	12 bits
QE peak	>45%
Full well capacity	>32,000 e-
Peak Signal to Noise Ratio	>400:1
Working distance	150 mm–¥
Field of View	31° X 31°
Field of View at 1 m distance	0.55 m X 0.55 m
Operational Temperature	0 C to +40 °C

© 2022, IJAAST All Rights Reserved, https://ijaast.com/

ISSN: 2348-1358
Impact Factor: 6.901
NAAS Rating: 3.77

Reflectance data up to 30% has been captured in the early phases of the disease deployment and can be used as spectral signatures for any future computation. Hyperspectral signatures for every class of gradation have been used to compare with that of different samples to prove the efficacy of the method and technology. Several constraints have been used to reduce the dimensionality of the data without hampering the loss in information and hence the loss in accuracy of identification. Since the wavelengths nest t each other are highly correlated, a spectral resolution of 7 nm has been used to differentiate during the analysis of the data. Single wavelengths are prioritized in calculating the specific range of disease among the severity.

The Specim IQ studio has been used as a tool to analyse the data between the extremes of reflectance of data wherein for a particular data, class segregation has been done during first indicative of the range of wavelengths to be identified for each of the respective classes. After plotting out the wavelengths of the nature of diseases about each class of severity, the image has been smoothed using the Savitzky-Golay algorithm and finally set to be run on other data as query templates during the image capture.

The Savitzky-Golay algorithm is a low pass filter, filtering out high frequencies and performing local polynomial regression in smoothing data since it maintains data instances such as impulse amplitude that generally degrade on moving through average. The equation can be found in Eq. 1 as follows.

$$g_i = \sum_{n-n_l}^{n_r} c_n f_{i+n} \qquad \text{…Eq. 1}$$

Where, g_i is the value that has been filtered at that position, i

f_j is the unfiltered value at that particular position, j

n_l focusses on the specification of data points on the left side of the point being smoothed

n_r focusses on the specification of data points on the right side of the point being smoothed

c_n is the weighting function

The process of data capture and measurement broadly involves five steps: At the time of setting up the establishment in capturing the camera through the spectrometer, the camera is to be directed towards the target using the viewfinder camera and a small vertical offset. Commonly used for any hyperspectral camera, a suitable homogeneous illumination is mandatory for getting a continuous spectrum of the wavelength pertaining to the range of interest. Specifically, the characteristics of illumination (through natural lighting or artificial halogen lamps) are analysed by using the white reference panel next to the target as discussed above.

After setting such equipment ready to go, the integration time is to be set and focus is to be adjusted by rotating the focus ring in getting the maximised focus of the target. The camera pre-set settings provide a default integration time but it can be adjusted manually between 1-500 ms. The parallax generated between the RGB camera or viewfinder camera and the primary camera is compensated upon calibration of the edges and its

© 2022, IJAAST All Rights Reserved, https://ijaast.com/

ISSN: 2348-1358
Impact Factor: 6.901
NAAS Rating: 3.77

detection between the viewfinder and focus rings. The parallax thus generated is adjusted to overlay between the viewfinder and spectral cameras with suitable accuracy.

With all such adjustments set up in attempting to capture an image, the shutter button is first half-pressed. With this, a new box inside the viewfinder appears including the small vertical offset in focus where after locking the integration time and finally full pressing the shutter button, the data is set to be captured following the method of line scanning through push-broom scanners.

After when the scanning gets completed, an image histogram is being set to account for any under or oversaturation of the data. Undersaturation is indicated by the blue colour in the histogram and oversaturation by red colour. The light intensity and the direction of focus of the illuminations play the primary role in setting up the saturation values after scanning the image. With no blue or red colour in the image histogram, the image is assumed to be correct with the environment settings, it is then accepted for being stored in the external storage and be used for further analysis.

With all the above process being completed, the white reference is being made to select by adjusting the spectral angle mapper (SAM) bar and then the image along with its spectral plot of reflectance vs. wavelength is being made to be able to see. With the image dimensions being 512 X 512 px, the spectral signature of any point over the image can be made see as a plot and any distortions of the same image can be identified by the distortion in the pattern of the spectral signature for that particular point.

The white reference can be used in pre-defined, simultaneous and custom white reference modes. In the first case, the camera and its memory set a general halogen spectrum from lower and outer threshold limits. In the second case, the white reference is used in the experiment itself to be set as per the illuminating conditions while in the last case, the white reference values can be set manually by the modes of custom selection. This selection can be set from any previous photo where the white reference has been used and identified.

3. Methodology

3.1 Hardware Workflow (Spectrometer)

The generalised steps for any hyperspectral image processing comprise of Radiometric Correction, Data Reduction for both spatial and spectral images, Endmember Selection between any target limits and eventually Hyperspectral Classification in which the material is identified and the targets are set to be fixed in detecting any objective, followed by Application-specific analysis at the fag end. The spectra have been selected from 675.73nm to 1000.49nm, which means it mainly pertains to the NIR range where the bands of wavelengths have been finely divided to produce better results (Fig 3).

© 2022, IJAAST All Rights Reserved, https://ijaast.com/

ISSN: 2348-1358
Impact Factor: 6.901
NAAS Rating: 3.77

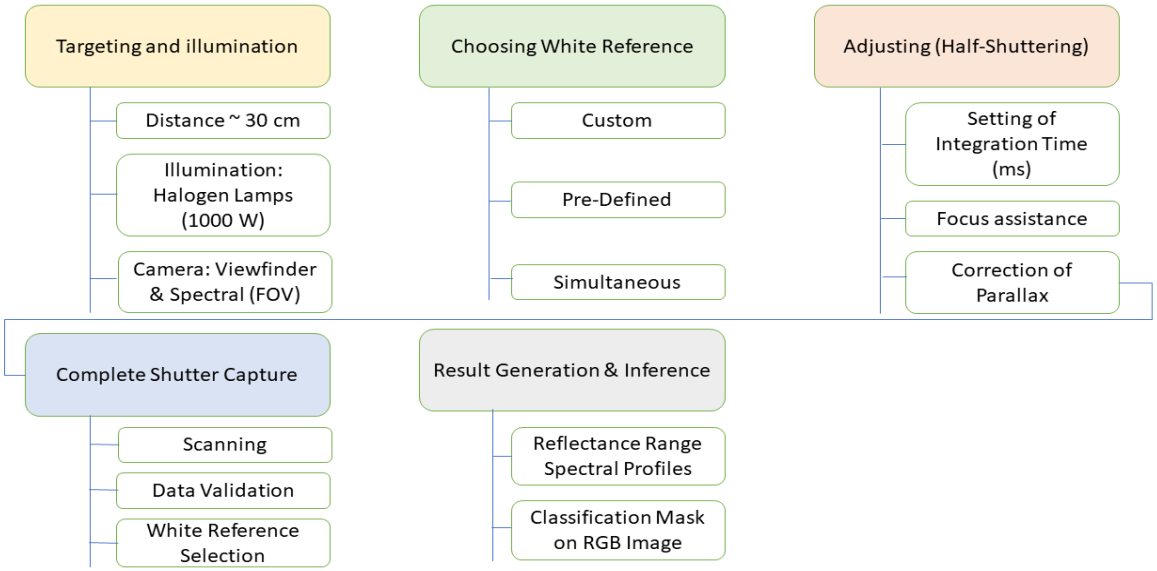

Fig 3.: Workflow using SpecimIQ Hyperspectral Camera

After when the image acquisition step gets over, in the image analysis step, the spectrometer provides three different modes, Default Recording Mode, Automatic Screening Mode and Application Mode.

In Default Recording Mode, the data cubes are stored separately consisting of all such raw and reflectance data. Such data are stored in the form of a folder structure where the information regarding the same is stored as meta information. In Automatic Screening Mode, the data cube thus captured is used to build a single class classifier and is based on Spectral Angle Mapper (Kruse et al., 1993). The user can select the reflectance spectra and the threshold for classifying data. The transformation of reflectance data is performed as described, prior to classification, and the selection of wavelength range is done to avoid using any such noisy areas in the spectra. The user has an option in building an application in the SpecimIQ studio software which can be deployed directly to the camera in capturing only the desired result. After incorporating the spectral library, the area is made to be selected containing the ROI in the image. The desired area containing the disease is made to be trained after smoothing and denoising using filters by Savitzky-Golay Algorithm (Savitzky & Golay, 1964). The specim studio software can be used where it allows the programmer to create a model, train it, create the spectral library and eventually the final deployment to the camera.

3.2 Software Workflow (Specim IQ Studio)

After when the image been captured using the spectrometer, it is stored and interfaced in the Specim IQ studio where different points showed different spectral signatures, the next step is to create a test model different spectral graphs are to be taken between the grade 0 (healthy leaf) and grade 1 (first onset of disease occurrence) may be noticed to predict the concept of early detection of such disease (Fig. 4).

© 2022, IJAAST All Rights Reserved, https://ijaast.com/

ISSN: 2348-1358
Impact Factor: 6.901
NAAS Rating: 3.77

The spectral angle mapper (SAM) matches the spectra of the particular pixel with the reference spectra for classifying the pixels. It calculates the angles between the spectra which have been considered as n-dimensional vectors in the space. The moderate success of this technique with classification accuracy of about 87% has made it popular in classifying the plant diseases. The selection of the area of interest has been proclaimed as the initial step in the software followed by the class identification of each grade to analyze the difference between the spectra for each. Spectra for points have been plotted in reflectance vs wavelength graph followed by masking as binary mask and eventually creating the application and deploying in the camera serves the purpose.

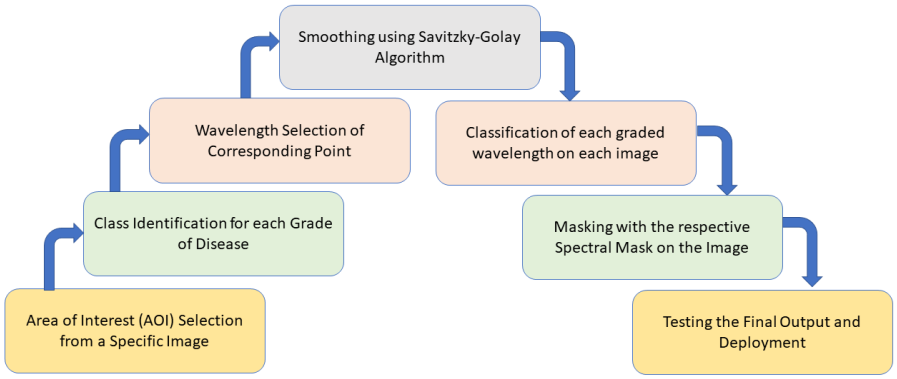

Fig. 4: Software Workflow of Data Analysis using Specim IQ Studio

The following table (Table 2) shows the steps pertaining to the spectral image processing and based on the parameters described here, the alterations and modifications are needed to be performed to predict a better result. However, optimized parts have been used in the processing of the image by the authors.

© 2022, IJAAST All Rights Reserved, https://ijaast.com/

ISSN: 2348-1358
Impact Factor: 6.901
NAAS Rating: 3.77

Table 2: Steps and selection of parameters during Spectral Image Processing

Steps on Pre-Processing	Image Types	Procedure	Advantages	Limitations
Dead Pixel	All types of images	Suppressed neighbour interpolation (Behrend et al., 2002; Cannistraci et al., 2009; Zhang & Henson, 2007)	Easier for implementation and calculation	If clustering of dead pixels is big, there is risk of losing resolution
	Hyperspectral and other multi bands	Thresholding based on detection of median spectra (Burger & Geladi, 2005)	Easier for implementation and calculation	High dependency on signal-to-noise ratio and risks on false positivity.
	All types but especially applicable for hyperspectral and multi-band images	Evolutionary algorithms based on genetic measures (Vankeerberghen et al., 1995)	Reliability and robustness	For finding the best combination of parameters in optimizing the fields
Spikes	Multi-Spectral Channels for a digital image	Selection criteria of wavelets (Ehrentreich & Sümmchen, 2001; Koshino et al., 2004)	Reliability and robustness	Proper Selection of wavelets in different types of images
	Multi-Spectral Channels for a digital image	Manual Inspection and detection of neighbouring filters (Behrend et al., 2002; Zhang & Henson, 2007)	Reliability and robustness	Excessive consumption of time, especially in case of hyperspectral images

© 2022, IJAAST All Rights Reserved, https://ijaast.com/

ISSN: 2348-1358
Impact Factor: 6.901
NAAS Rating: 3.77

	Multi-Spectral Channels for a digital image	Suppressed neighbour interpolation (Ehrentreich & Sümmchen, 2001; Koshino et al., 2004; Zhang & Henson, 2007)	Easier for implementation and calculation	Difficulty for finding the exact threshold
Background region of interest	All	Principal Component Analysis thresholding (Burger & Geladi, 2005)	Robustness in selection of a specified area	Non-obvious and tedious selection of proper threshold
Spectral Pre-Processing	Hyperspectral Images (Especially)	Smoothing by Savitzky-Golay, denoising and correction in scattering (Amigo, 2010)	Easy for Implementation	Finding the best parameters combination in optimizing the filter
Compression	All	Encoding of Bytes (Schmalzl, 2003)	Efficiency in compression	Specific types of Images, pertaining to the software compatibility
	All, especially hyperspectral ones	Binned Spectra (Srinivas & Wilson, 2004)	Easy for Implementation	Loss in spectral resolution

© 2022, IJAAST All Rights Reserved, https://ijaast.com/

ISSN: 2348-1358
Impact Factor: 6.901
NAAS Rating: 3.77

	All, especially hyperspectral ones	Binned Space (Srinivas & Wilson, 2004)	Easy for Implementation	Loss in spectral resolution
	All, especially hyperspectral ones	Factor Models (Juan et al., 2014)	Easy for Implementation	Loss in spectral resolution
	All, especially hyperspectral ones	Wavelets (Gao & Yan, 2010)	Easy for Implementation	Loss in spectral resolution

Based on the supporting steps and mechanisms in processing the spectral images it becomes easier in achieving the objectives of the work and has been elaborated in the results and discussion (Section 4).

4. Results and Discussion

The early-stage detection through spectral differences has a number of implications:

i) The chlorophyll content on the leaf can be analysed and estimated.
ii) The reflectance spectrum for the same leaf at two different point of time shows the probability of onset of pathogens.
iii) The ability of the leaf to be photosynthesized gets known based upon such parameters of reflectance and transmittance.

The calculation of chlorophyll is based on Eq. 2 and is generally done by biochemical laboratories. This experiment has not been done by the authors and is thus presented as an implication in adding a parameter for predicting the onset of diseases. However, this has not been an objective for the researchers through the demand of the project being worked upon.

$$\text{Chlorophyll a (mg/mL)} = 12.7\,\lambda663 - 2.69\,\lambda645$$
$$\text{Chlorophyll b (mg/mL)} = 22.9\,\lambda645 - 4.68\,\lambda663 \quad \ldots\text{Eq. 2}$$

where:
$\lambda645$ = absorbance at a wavelength of 645 nm;
$\lambda663$ = absorbance at a wavelength of 663 nm.

The following figure (Fig. 5) depicts the graph for the corresponding healthy leaf and Fig 6 depicts the graph for the leaf with the first slightest occurrence of the disease. The difference in the reflectance vs wavelength

© 2022, IJAAST All Rights Reserved, https://ijaast.com/

ISSN: 2348-1358
Impact Factor: 6.901
NAAS Rating: 3.77

graph shows the onset of diseases on the leaf and one may notice that as there is a slightest onset of disease, the reflectance values lower as Fig 2 showed that the unhealthy leaves' reflectance spectra is lowered that the healthy ones.

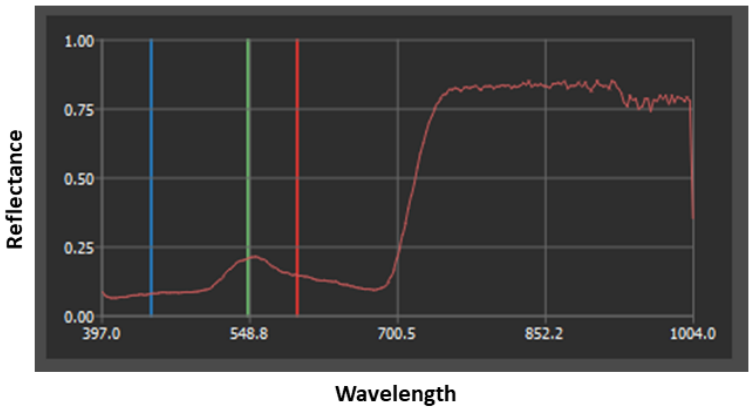

Fig. 5: Spectral graph for the healthy leaf

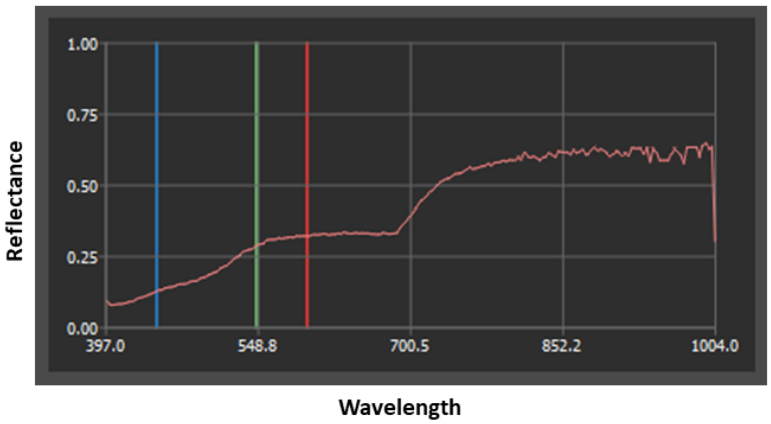

Fig. 6: Spectral graph for the leaf with slightest probability about onset of pathogens

As one can notice the difference in spectra in the adjoining graphs and can conclude that with such hyperspectral cameras and technologies for analysis, one can realistically hope in identifying nonvisual symptoms and save the crops from ultimate devastation. One popular technique in particular is Simplex Volume Maximisation (Lowe et al., 2017) in early detection of any sort of stress in plants, where spectral signatures are taken from samples of diseased and healthy images of plants. These signatures are then clustered in separate classes and on a query image; a matching operation is performed to classify the new signature based on the classes clustered.

© 2022, IJAAST All Rights Reserved, https://ijaast.com/

ISSN: 2348-1358
Impact Factor: 6.901
NAAS Rating: 3.77

Table 3 depicts the average reflectance values from the images of the leaves having disease graded from 1-9 using the Savitzky – Golay derivative of partial least square regression.

Table 3: Average Reflectance values for different graded leaves

Grades	Average Reflectance Values
0	0.796
1	0.652
2	0.621
3	0.578
4	0.569
5	0.482
6	0.463
7	0.452
8	0.412
9	0.378

Based on the datasets, the technology has been required to be calibrated based on the readings of the known components. The associated validation and calibration parameters have been shown in Table 4. The significance of PLS models can be observed with p-values < 0.0001. The range of R^2 from 0.96 to 0.993 shows good calibration and validation statistics with Root Mean Square Error (RMSE) values from 3.01 to 5.95% and 2.65 to 5.98% respectively.

Table 4: Calibration and Validation Statistics of PLS

Cycle	Intercept	Slope	RMSE (%)	SE (%)	Bias (%)	R^2	p-value	RPD	N
Calibration									
S1	0.2698	0.9832	2.6339	2.5682	1.34E-07	0.983	0.0001	12.2	105
S2	0.2347	0.9827	2.6525	2.6569	-6.52E08	0.987	0.0001	5.2	22.1
S3	0.2487	0.9863	2.4878	2.7895	-5.65E09	0.879	0.0001	5.8	16.9

© 2022, IJAAST All Rights Reserved, https://ijaast.com/

ISSN: 2348-1358
Impact Factor: 6.901
NAAS Rating: 3.77

Validation									
S1	0.2587	0.9765	2.5163	2.8759	-6.24E07	0.985	0.0001	6.4	17.2
S2	0.2462	0.9814	2.6254	2.8965	5.47E03	0.9765	0.0001	7.1	18.6
S3	0.2568	0.9952	2.2145	2.9658	6.52E08	0.9862	0.0001	8.4	17.9

The technology has been observed in more than 250 healthy leaves where disease onset has been done both naturally and artificially and the results of early detection has been validated by the plant pathologists based on the difference in spectra. Thus, from the experimental value and validation from the plant pathologists, the range of grades pertaining to the quantification of the severity can be estimated (Fig. 7).

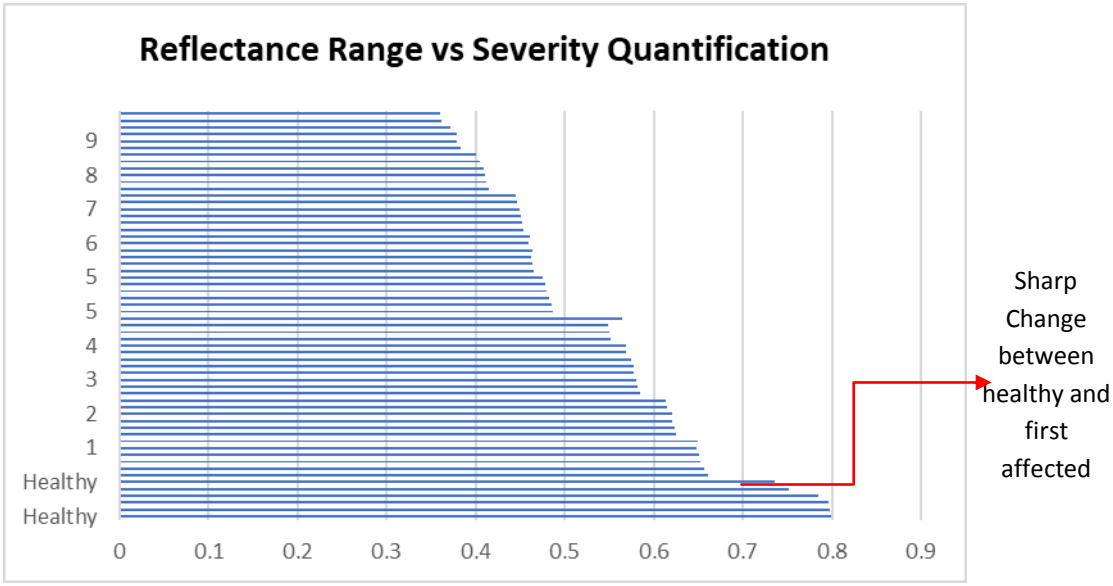

Fig.7: Reflectance range vs the severity quantification of the disease on a spectral graph

4.1 Disease Severity Quantification

The quantification on the severity of the diseases affecting the leaves can be estimated from Table 3 based on the gradation of the leaves. Extreme damage through the disease can deterministically affect the appearance of the leaves which may eventually lead to discard it from the plant itself. However, Spectral Angle Mapper approach can be used to classify these pixels through the calculation of the angles between the pixel spectra and reference spectra (Lowe et al., 2017). It is based on the following equation (Eq. 2):

© 2022, IJAAST All Rights Reserved, https://ijaast.com/

ISSN: 2348-1358
Impact Factor: 6.901
NAAS Rating: 3.77

$$\cos^{-1}\frac{\sum_{i=1}^{nb} x_i y_i}{\sqrt{\sum_{i=1}^{nb} x_i^2}\sqrt{\sum_{i=1}^{nb} y_i^2}} \quad \text{…Eq. 2}$$

Where, x_i is the test spectrum, y_i is the reference spectrum and nb is the total number of bands

5. Conclusion

Each and every developed spectral disease index help in identifying the spectral diseases but becomes difficult at an earlier stage of detection due to less variation in the leaf reflectances. The use of Specim IQ handheld hyperspectral camera, capable of taking information of the area of interest from 400 to 1000 nm of wavelength has been seen as a boon in developing a non-invasive identification of diseases through the measurement of Normalized Different Vegetation Index and Photochemical Reflectance Index from the images. The result thus obtained from the vegetation indices impart huge application in the research area of plant phenotyping strategies. In assessing downy mildew, Specim IQ proves to be a promising device in capturing information from the respective wavelength bands and in addition to the use of Simplex Volume Maximization, Partial Least Squares and other denoising filters in addition to end member selection, the analysis becomes more proficient in inferring to any conclusion regarding the onset and confirmation of diseases. The trade-off between the data quality, throughput and stability in pertaining environmental conditions proves to be a promising device in not only capturing information but also developing suitable application models in predicting the early detection and severity of the diseases through grades from the affected ones. Future work would certainly include deploying the application into the device in testing the scalability and precision a time saving and reproducible disease monitoring system for early detection of diseases in the targeted plant.

Acknowledgement

The authors would also like to thank Dr. A. Bandyopadhyay, Senior consultant, ITRA Ag&Food and Dr. Sourabh Kumar Das, Principal, Kalyani Government Engineering College, for helping us to implement this research work.

Declarations

Conflict of interest

The authors declare no conflicts of interest regarding publication of this paper.

Funding Source:

The authors would like to thank to Science and Engineering Research Board (SERB), Government of India, File No. EEQ/2018/001074 (Ver-1) dated 10 October, 2018 for funding this research work.

Contributions

Subhranil Mustafi: Original Writing and Partial Idea Generation, Shubhajyoti Das: Literature Analysis, Kunal Roy: On Field Experimentation of Proposed Methodology, Sanket Dan: Conceptualization of Proposed Methodology & Satyendra Nath Mandal: Guidance of the complete process

© 2022, IJAAST All Rights Reserved, https://ijaast.com/

ISSN: 2348-1358
Impact Factor: 6.901
NAAS Rating: 3.77

Informed consent

Informed consent has been obtained from all the co-authors.

References

[1]. Ahmed, M. R., Yasmin, J., Mo, C., Lee, H., Kim, M. S., Hong, S.-J., & Cho, B.-K. (2016). Outdoor Applications of Hyperspectral Imaging Technology for Monitoring Agricultural Crops: A Review. *Journal of Biosystems Engineering*, *41*(4), 396–407. https://doi.org/10.5307/jbe.2016.41.4.396

[2]. Amigo, J. M. (2010). Practical issues of hyperspectral imaging analysis of solid dosage forms. *Analytical and Bioanalytical Chemistry*, *398*(1), 93–109. https://doi.org/10.1007/s00216-010-3828-z

[3]. Behmann, J., Acebron, K., Emin, D., Bennertz, S., Matsubara, S., Thomas, S., Bohnenkamp, D., Kuska, M. T., Jussila, J., Salo, H., Mahlein, A. K., & Rascher, U. (2018). Specim IQ: Evaluation of a new, miniaturized handheld hyperspectral camera and its application for plant phenotyping and disease detection. *Sensors (Switzerland)*, *18*(2). https://doi.org/10.3390/s18020441

[4]. Behrend, C. J., Tarnowski, C. P., & Morris, M. D. (2002). Identification of Outliers in Hyperspectral Raman Image Data by Nearest Neighbor Comparison. *Applied Spectroscopy*, *56*(11), 1458–1461. https://doi.org/10.1366/00037020260377760

[5]. Blackburn, G. A. (1998). Quantifying Chlorophylls and Caroteniods at Leaf and Canopy Scales: An Evaluation of Some Hyperspectral Approaches. *Remote Sensing of Environment*, *66*(3), 273–285. https://doi.org/https://doi.org/10.1016/S0034-4257(98)00059-5

[6]. Bravo, C., Moshou, D., West, J., McCartney, A., & Ramon, H. (2003). Early disease detection in wheat fields using spectral reflectance. *Biosystems Engineering*, *84*(2), 137–145. https://doi.org/10.1016/S1537-5110(02)00269-6

[7]. Burger, J., & Geladi, P. (2005). Hyperspectral NIR Image Regression Part I: Calibration and Correction. *Journal of Chemometrics*, *19*, 355–363. https://doi.org/10.1002/cem.938

[8]. Caballero, D., Calvini, R., & Amigo, J. M. (2020). Hyperspectral imaging in crop fields: precision agriculture. *Data Handling in Science and Technology*, *32*, 453–473. https://doi.org/10.1016/B978-0-444-63977-6.00018-3

[9]. Cannistraci, C. V, Montevecchi, F. M., & Alessio, M. (2009). Median-modified Wiener filter provides efficient denoising, preserving spot edge and morphology in 2-DE image processing. *Proteomics*, *9*(21), 4908–4919. https://doi.org/10.1002/pmic.200800538

[10]. Darvishzadeh, R., Matkan, A. A., & Dashti Ahangar, A. (2012). Inversion of a radiative transfer model for estimation of rice canopy chlorophyll content using a lookup-table approach. *IEEE Journal of Selected Topics in Applied Earth Observations and Remote Sensing*, *5*(4), 1222–1230. https://doi.org/10.1109/JSTARS.2012.2186118

[11]. Doraiswamy, P., Moulin, S., Cook, P., & Stern, A. (2003). Crop Yield Assessment from Remote Sensing. *Photogrammetric Engineering & Remote Sensing*, *69*, 665–674. https://doi.org/10.14358/PERS.69.6.665

[12]. Ehrentreich, F., & Sümmchen, L. (2001). Spike Removal and Denoising of Raman Spectra by Wavelet Transform Methods. *Analytical Chemistry*, *73*(17), 4364–4373. https://doi.org/10.1021/ac0013756

[13]. Fong, A. Y., & Wachman, E. (2008). Hyperspectral imaging for the life sciences. *Biophotonics International*, *15*(3), 38–41.

[14]. Galvão, L. S., Roberts, D. A., Formaggio, A. R., Numata, I., & Breunig, F. M. (2009). View angle effects on the discrimination of soybean varieties and on the relationships between vegetation indices and yield using off-nadir Hyperion data. *Remote Sensing of Environment*, *113*(4), 846–856. https://doi.org/https://doi.org/10.1016/j.rse.2008.12.010

[15]. Gao, R., & Yan, R. (2010). Wavelets: Theory and Applications for Manufacturing. In *Wavelets:*

© 2022, IJAAST All Rights Reserved, https://ijaast.com/

ISSN: 2348-1358
Impact Factor: 6.901
NAAS Rating: 3.77

Theory and Applications for Manufacturing. https://doi.org/10.1007/978-1-4419-1545-0

[16]. Gitelson, A. A., Kaufman, Y. J., Stark, R., & Rundquist, D. (2002). Novel algorithms for remote estimation of vegetation fraction. *Remote Sensing of Environment*, *80*(1), 76–87. https://doi.org/https://doi.org/10.1016/S0034-4257(01)00289-9

[17]. Gonzalez-Dugo, V., Hernandez, P., Solis, I., & Zarco-Tejada, P. J. (2015). Using high-resolution hyperspectral and thermal airborne imagery to assess physiological condition in the context of wheat phenotyping. *Remote Sensing*, *7*(10), 13586–13605. https://doi.org/10.3390/rs71013586

[18]. Hatfield, J. L., Gitelson, A. A., Schepers, J. S., & Walthall, C. L. (2008). Application of spectral remote sensing for agronomic decisions. *Agronomy Journal*, *100*(3 SUPPL.). https://doi.org/10.2134/agronj2006.0370c

[19]. Hruska, R., Mitchell, J., Anderson, M., & Glenn, N. F. (2012). Radiometric and geometric analysis of hyperspectral imagery acquired from an unmanned aerial vehicle. *Remote Sensing*, *4*(9), 2736–2752. https://doi.org/10.3390/rs4092736

[20]. Huang, W., Lamb, D. W., Niu, Z., Zhang, Y., Liu, L., & Wang, J. (2007). Identification of yellow rust in wheat using in-situ spectral reflectance measurements and airborne hyperspectral imaging. *Precision Agriculture*, *8*(4), 187–197. https://doi.org/10.1007/s11119-007-9038-9

[21]. Juan, A. de, Piqueras, S., Maeder, M., Hancewicz, T., Duponchel, L., & Tauler, R. (2014). Chemometric Tools for Image Analysis. In *Infrared and Raman Spectroscopic Imaging* (pp. 57–110). John Wiley & Sons, Ltd. https://doi.org/https://doi.org/10.1002/9783527678136.ch2

[22]. Koshino, K., Zuo, H., Saito, N., & Suzuki, S. (2004). Improved spike noise removal in the scanning laser microscopic image of diamond abrasive grain using wavelet transforms. *Optics Communications*, *239*(1), 67–78. https://doi.org/https://doi.org/10.1016/j.optcom.2004.05.056

[23]. Kruse, F. A., Lefkoff, A. B., Boardman, J. W., Heidebrecht, K. B., Shapiro, A. T., Barloon, P. J., & Goetz, A. F. H. (1993). The spectral image processing system (SIPS)-interactive visualization and analysis of imaging spectrometer data. *Remote Sensing of Environment*, *44*(2–3), 145–163. https://doi.org/10.1016/0034-4257(93)90013-N

[24]. Lodhi, V., Chakravarty, D., & Mitra, P. (2019). Hyperspectral Imaging System: Development Aspects and Recent Trends. *Sensing and Imaging*, *20*(1). https://doi.org/10.1007/s11220-019-0257-8

[25]. Lowe, A., Harrison, N., & French, A. P. (2017). Hyperspectral image analysis techniques for the detection and classification of the early onset of plant disease and stress. *Plant Methods*, *13*(1), 1–12. https://doi.org/10.1186/s13007-017-0233-z

[26]. Lu, B., Dao, P. D., Liu, J., He, Y., & Shang, J. (2020). Recent advances of hyperspectral imaging technology and applications in agriculture. *Remote Sensing*, *12*(16), 1–44. https://doi.org/10.3390/RS12162659

[27]. Lucieer, A., Malenovský, Z., Veness, T., & Wallace, L. (2014). HyperUAS - Imaging spectroscopy from a multirotor unmanned aircraft system. *Journal of Field Robotics*, *31*(4), 571–590. https://doi.org/10.1002/rob.21508

[28]. Mahlein, A. K., Oerke, E. C., Steiner, U., & Dehne, H. W. (2012). Recent advances in sensing plant diseases for precision crop protection. *European Journal of Plant Pathology*, *133*(1), 197–209. https://doi.org/10.1007/s10658-011-9878-z

[29]. Penuelas, J., Baret, F., & Filella, I. (1995). Semi-empirical indices to assess carotenoids/chlorophyll a ratio from leaf spectral reflectance. *Photosynthetica*, *31*(2), 221–230.

[30]. PEÑUELAS, J., FILELLA, I., BIEL, C., SERRANO, L., & SAVÉ, R. (1993). The reflectance at the 950–970 nm region as an indicator of plant water status. *International Journal of Remote Sensing*, *14*(10), 1887–1905. https://doi.org/10.1080/01431169308954010

[31]. Rouse J.~W., J., Haas, R. ~H., Schell, J. ~A., & Deering, D. ~W. (1974). Monitoring Vegetation Systems in the Great Plains with Erts. In *NASA Special Publication* (Vol. 351, p. 309).

[32]. Savitzky, A., & Golay, M. J. E. (1964). Smoothing and Differentiation of Data by Simplified Least Squares Procedures. *Analytical Chemistry*, *36*(8), 1627–1639. https://doi.org/10.1021/ac60214a047

[33]. Schmalzl, J. (2003). Using standard image compression algorithms to store data from computational

© 2022, IJAAST All Rights Reserved, https://ijaast.com/

ISSN: 2348-1358
Impact Factor: 6.901
NAAS Rating: 3.77

fluid dynamics. *Computers & Geosciences*, *29*, 1021–1031. https://doi.org/10.1016/S0098-3004(03)00098-0

[34]. Srinivas, Y., & Wilson, D. (2004). Quantitative image quality evaluation of pixel-binning in a flat-panel detector for x-ray fluoroscopy. *Medical Physics*, *31*, 131–141. https://doi.org/10.1118/1.1628278

[35]. Steddom, K., Bredehoeft, M. W., Khan, M., & Rush, C. M. (2005). Comparison of visual and multispectral radiometric disease evaluations of Cercospora leaf spot of sugar beet. *Plant Disease*, *89*(2), 153–158. https://doi.org/10.1094/PD-89-0153

[36]. Taylor, A. S., & Cook, D. C. (2018). An economic assessment of the impact on the Western Australian viticulture industry from the incursion of grapevine downy mildew. *Journal of Plant Diseases and Protection*, *125*(4), 397–403. https://doi.org/10.1007/s41348-018-0152-x

[37]. Thenkabail, P. S., Smith, R. B., & De Pauw, E. (2000). Hyperspectral Vegetation Indices and Their Relationships with Agricultural Crop Characteristics. *Remote Sensing of Environment*, *71*(2), 158–182. https://doi.org/https://doi.org/10.1016/S0034-4257(99)00067-X

[38]. Transon, J., d'Andrimont, R., Maugnard, A., & Defourny, P. (2018). Survey of hyperspectral Earth Observation applications from space in the Sentinel-2 context. *Remote Sensing*, *10*(2), 1–32. https://doi.org/10.3390/rs10020157

[39]. Vankeerberghen, P., Smeyers-Verbeke, J., Leardi, R., Karr, C. L., & Massart, D. L. (1995). Robust regression and outlier detection for non-linear models using genetic algorithms. *Chemometrics and Intelligent Laboratory Systems*, *28*(1), 73–87. https://doi.org/https://doi.org/10.1016/0169-7439(95)80041-7

[40]. Zhang, L., & Henson, M. J. (2007). A Practical Algorithm to Remove Cosmic Spikes in Raman Imaging Data for Pharmaceutical Applications. *Applied Spectroscopy*, *61*(9), 1015–1020. https://doi.org/10.1366/000370207781745847

Authors:

Satyendra Nath Mandal completed his Ph.D. from Maulana Abul Kalam Azad University of Technology, Kolkata, India and is currently an Assistant Professor in the Department of Information Technology of Kalyani Government Engineering College. He has authored more than 100 Research Papers including Conferences and Journals and is currently a Principal Investigator in a number of Government Funded Research Projects.

Subhranil Mustafi completed his M.Tech in Information Technology from Kalyani Government Engineering College in 2020. He qualified Graduate Aptitude Test in Engineering (GATE) in 2018. He is a Gold Medalist in Information Technology from MAKAUT, WB, India. He has authored more than 10 research papers and articles in 2020 and currently working in the domain of animal identification. He received the Best Student Project Award for the final year Research Project in B.Tech in Ani-mal Identification. His research interest lies in Digital Image Processing (extensively in the area of Biometric Identification), Internet of Things and Data Science.

Shubhajyoti Das did his Masters in Information Technology from Kalyani Government Engineering College and is currently working as a Project Assistant at Kalyani Government Engineering College. His research interests lie in Machine Learning and Computer Vision and has con-tributed extensively in the areas of Smart Farming, Plant Disease Identification and Classification.

Sanket Dan completed his M.Tech in Information Technology from Kalyani Government Engineering College and is currently the Rajiv Gandhi National Fellow for pursuing Ph.D. in Computer Science and Engineering. He has an Intellectual Property Certification for copyrighting Individual Pig Identification using Biometrics.

© 2022, IJAAST All Rights Reserved, https://ijaast.com/